J. Fluid Mech. (1973), *vol.* 61, *part* 4, *pp.* 731–751
Printed in Great Britain

Experiments on instability and turbulence in a stratified shear flow

By S. A. THORPE

Institute of Oceanographic Sciences, Wormley, Godalming, Surrey

(Received 23 May 1973)

This is a study of turbulence which results from Kelvin–Helmholtz instability at the interface between two miscible fluids in a two-dimensional shear flow in the laboratory. The growth of two-dimensional 'billows', their disruption by turbulence, and the eventual decay of this turbulence and the re-establishment of a gravitationally and kinematically stable interface are described. Continuous measurements of density and horizontal velocity from both fixed and vertically moving probes have been made, and the records obtained are presented, together with photographs showing the simultaneous appearance of the flow, which serve to identify the physical nature of events seen in the records. The measurements show how the fine-structure of the density field described in earlier experiments is related to velocity fluctuations. The vertical length scales of the final mean velocity and density structure are found to be different, and to depend on the Richardson number at which instability first occurred. The eventual Richardson number at the centre of layer is, however, not dependent on the initial Richardson number and has a value of about one third. The implications of these results to the eddy diffusion coefficients, to the energy exchange, and to turbulence in the ocean and the atmosphere are discussed.

1. Introduction

Observations of motion in stably stratified fluids reveal that turbulence is often sporadic; it occurs in bursts of relatively high intensity in an environment in which changes are gradual, in which small-amplitude internal waves dominate the motion. Measurements from a submarine in the ocean thermocline by Grant, Moilliet & Vogel (1968) showed that irregular high-frequency fluctuations of temperature and velocity, symptomatic of turbulence, occurred in only a small percentage of the volume, and visual observations by divers (Woods 1968) have shown that turbulence can arise in patches as the result of locally overturning 'billows' (resembling a two-dimensional structure in which the lines of constant density are distorted into spirals, each with a horizontal axis in the same plane and all with the same sense of rotation, rather like the cats-eye structure described by Kelvin). These are induced by passing internal gravity waves and last for about a minute or two. Other examples of irregular fluctuations over small vertical scales have been documented by Gregg & Cox (1972), who used a freely falling instrument to record both temperature and salinity on scales of the order of 1 cm in the ocean. Some of these fluctuations may result from their instrument

falling through 'billows' or the turbulence which follows them, but it is probable that double-diffusive convection or rotors occurring in breaking internal waves may account for some of the irregularity in their profiles of temperature and salinity. Considerable advances in the study of atmospheric turbulence have been made with the use of high-powered short-wavelength radar which can detect the weak scattering from temperature gradients (or, at low levels, relative humidity gradients) on a scale of a few centimetres. Browning (1971) and others have detected atmospheric structures with this facility which resemble the thermocline billows. Atmospheric billows are observed to develop on a time scale of about 5 min, although their effects persist for much longer periods. Their shape, as measured by the ratio s of their maximum height to wavelength, is not constant but varies from one sighting to another. Browning's observations give

$$0{\cdot}097 < s < 0{\cdot}500.$$

Recent measurements have combined remote radar detection with *in situ* measurements from aircraft (Hardy, Reed & Mather 1973; Browning *et al.* 1973) or from instruments supported by tethered balloons (Readings, Golton & Browning 1973), and these provide horizontal or time profiles of temperature and wind speed in, or close to, the billow structures.

There is now considerable evidence that the observed billows result from a shear-induced instability in a gravitationally stably stratified fluid, frequently called Kelvin–Helmholtz instability. The thermocline billows result from the increased local shear caused by internal gravity waves, and the atmospheric billows are often caused in the same way or by locally accelerated flow over the top of a rising thermal (as in the case studied by Readings *et al.*) or in low Richardson number regions in fronts (Browning, Harrold & Starr 1970). The turbulence associated with the billow structure is thought to be a frequent cause of clear-air turbulence in the upper troposphere and lower stratosphere (Roach 1972). It is therefore important to understand how it is generated, and if possible, to predict its onset. The billows may also be important, both in the atmosphere and in the ocean, in that they contribute significantly to vertical transports of momentum and heat (or solutes) and that they create a density microstructure when they collapse. Garrett & Munk (1972) have investigated the importance of this mixing process by internal wave-induced shear in the ocean.

Laboratory experiments and theories of turbulence in stably stratified fluids have mostly been concerned with continuously maintained turbulence, and the atmospheric boundary layer has often been the object of investigations. Turner (1973, chapters 5 and 9) describes several studies of maintained turbulence, and Cermak & Arya (1970) have also reviewed work in this field. The observations in the ocean and atmosphere suggest, however, that a more appropriate model is one in which Kelvin–Helmholtz instability and weak turbulence occasionally occur as the result of some local intensification of the shear, and that the turbulence then decays, perhaps radiating internal waves which themselves trigger instability in another, more sensitive, part of the fluid. This weak turbulence *may* be regarded as a slowly decaying form of a maintained and continuous turbulence, or perhaps as a description of the motion some distance from a source

of maintained turbulence, and driven primarily by radiating internal waves. The understanding of such weak, or intermittent, turbulence may be guided by this account of a simple experiment in which a single Kelvin–Helmholtz instability event (wave growth, billow development, turbulence and decay) is followed; weak turbulence may be regarded as an ensemble of such events, interacting only in so far as one may trigger another in the manner suggested.†

The experiment is a continuation of a series which has been described previously (Thorpe 1968, 1971, 1973, referred to as I, II, III, respectively, in the account which follows). A long closed tube is completely filled with a layer of brine lying under a layer of water. Diffusion between the two layers results in a profile of density which closely approximates to an error function. A nearly parallel, uniformly accelerating shear flow is set up by tilting the tube through a small angle; the gradient Richardson number in the flow decreases as $1/t^2$ (t is the time). When the required Richardson number is reached, the tube is returned to a level position. The flow in the centre is thereafter uniform and parallel to the tube walls, except for the influence of viscosity and the eventual arrival of surges from the ends of the tube or, as of course is the object of the experiment, by the growth of waves which result from Kelvin–Helmholtz instability. These waves grow and undergo a roll-up, in which the spirals (the billows) form at alternate nodes. The interfaces between the billows are markedly thinner than the original interface, thinner than can be accounted for by simple stretching, indicating a flow and transport of fluid from these regions into the billows. Indeed this development of large gradients between billows is a remarkable feature of the instability. The wave growth is reduced after the formation of the billows, and a secondary instability occurs in which small-scale structure and three-dimensional motions are generated in the billows. The billows extend horizontally and amalgamate to form a layer of turbulence, which then thickens, the irregular motion decreases in magnitude, vertical stable gradients are re-established and turbulence decays, leaving a thickened interface clouded with a fine structure of almost horizontal saline elements (figure 1, plates 1 and 2). These experiments with unstratified fluid outside the initial interface do not allow the escape of energy by vertically propagating internal waves. (We have estimated the importance of this effect in III.) It is thus possible to examine the initial and final energy of the mean flow and to estimate how much energy has been lost. We shall be concerned with the net energy exchange, and particularly with the role played by the initial Richardson number.

2. Theory

We consider a stratified inviscid fluid of density

$$\rho = \rho_0(1 - \Delta \operatorname{erf} \beta z), \tag{1}$$

where ρ_0, β and Δ ($\ll 1$) are constant, confined in a long rectangular tube with vertical sides and with upper and lower walls, at $z = \pm H$, inclined at an angle α

† This model should also include the possibility of rotor formation in breaking internal waves (Orlanski & Brian 1969; Orlanski 1972; Frankignoul 1972) although Garrett & Munk (1972) show that shear instability is much more likely in the ocean.

to the horizontal at time $t = 0$, when the fluid begins its motion from rest. The thickness of the density interface will be defined as $\sqrt{\pi}/\beta$, a quantity which can easily be calculated from the measured density profiles of the experiments, by drawing a line which represents the gradient at $z = 0$ and by measuring the vertical distance between the intercepts of this line and the (extended) lines $\rho = \rho_0(1 \pm \Delta)$. This method was used to measure the thickness of both density and velocity interfaces, and is used as a definition of the thickness in this paper. The subsequent flow in the centre of the tube is parallel to the walls and is given by

$$u = g\Delta t \sin\alpha \operatorname{erf}\beta z \tag{2}$$

(see I). If at time t_0 the tube is suddenly brought into a horizontal position, the flow near the centre continues with a speed

$$u(z) = g\Delta t_0 \sin\alpha \operatorname{erf}\beta z = U_0 \operatorname{erf}\beta z, \quad \text{say,} \tag{3}$$

unless instability occurs or until the flow is interrupted by the arrival of surges from the ends of the tube. The minimum gradient Richardson number in the flow is

$$R_I = g\Delta\sqrt{\pi}/2\beta U_0^2 \tag{4}$$

at $z = 0$, and it is this parameter which determines whether or not the flow is stable.

In practice fluids are viscous, and although the velocities in parts of the tube remote from $z = 0$ and the tube walls are found to be well predicted by (3), the velocity gradient at $z = 0$ is reduced by a factor

$$Q = \frac{2}{1 + [1 + 8\beta(\nu t)^{\frac{1}{2}}/\pi]^{\frac{1}{2}}}, \tag{5}$$

where ν is the kinematic viscosity (see II). The thickness of the velocity interface at $t = t_0$ is thus $\sqrt{\pi}/(\beta Q)$ and the Richardson number R_I is increased by a factor $1/Q^2$.

The growth of wavelike disturbances resulting from Kelvin–Helmholtz instability may begin when the minimum gradient Richardson number falls below a quarter. In the present experiments it was arranged that the waves had values of s (the wave height divided by wavelength) less than 0·1 and usually much less, at t_0, and thus did not seriously affect the flow at this time. To achieve these conditions at the small values of R_I it was necessary to have as large angles of tilt α as possible, without making the time taken to tilt the tube long in comparison with the time that it remained stationary in an inclined position. As can be seen from II (figure 3), the larger the angle of tilt, the smaller is the value of the Richardson number obtained before the amplitude of the disturbance has increased by a given fraction. We also attempted to reduce the influence of viscosity by completing each experiment in the shortest possible time. This was achieved by using fairly large values of Δ. There were other physical limitations on the experiment. We used the longest (4·85 m) tube which could easily be constructed, accommodated and yet easily tilted, so as to allow as much time as possible to pass before the surges from the ends of the tank arrive at the centre. The tube height (16 cm) was

a compromise; if it is too small the upper and lower boundaries affect the turbulent layer, whilst the greater the height the faster is the speed of the surges. (Their speed depends also on Δ.) The billow amplitude and final thickness of the turbulent region are, as we shall show later, related to R_I and the thickness of the density interface, and given the tube height, the range of useful interface thicknesses is limited.

We shall suppose that the development of the waves after the tube has been returned into a horizontal position is not dependent upon the way in which the flow was set up. We therefore parameterize the subsequent motion using the Richardson number R_I (as defined by (4) and modified by $1/Q^2$), Q and a Reynolds number

$$R_e = 2U_0\sqrt{\pi}/\nu\beta Q$$

and non-dimensionalize using U_0, $g\Delta$, ν and κ (the molecular diffusivity of salt; ν and κ are supposed to be constant), but *not* using, for example, the angle of tilt α, or the time t_0, or the spectrum of the disturbances within the tube at t_0. It is implicit in this assumption that the motion at t_0 is not so dominated by the history of the flow that it retains this information about its past at the later time when the instability reaches large amplitude and the flow undergoes a transition to turbulence. A convenient time scale which will be used in describing the turbulent motion is $U_0/g\Delta$; $\tau = tg\Delta/U_0$ will be used to give a non-dimensional measure of the time t elapsed since the first appearance of fine-structure in the density field within the billows. The Richardson number $g\Delta L/U_0^2$ will be used as a non-dimensional measure of a vertical length L.

The experiments were made in the parameter ranges

$$0{\cdot}04 < R_I < 0{\cdot}20, \quad 0{\cdot}72 < Q < 0{\cdot}93,$$
$$0{\cdot}01 < \Delta < 0{\cdot}065, \quad 1400 < R_e < 12\,000,$$

with values of ν and κ taken as $0{\cdot}01$ and $1{\cdot}43 \times 10^{-5}\,\mathrm{cm\,s^{-2}}$ respectively. The Prandtl number ν/κ has not been varied and some effects (see Turner 1973, chapter 9), and particularly the persistence of fine-structure, might depend on this value. The experiments of Moore & Long (1971), suggest, however, that the major conclusions of this paper will not be affected by the actual Prandtl number used. Typical values of U_0 and $\sqrt{\pi}/\beta$ were $10\,\mathrm{cm\,s^{-1}}$ and $1{\cdot}5\,\mathrm{cm}$ respectively.

3. Observations

3.1. *Measurements*

The experiments were recorded by both still and ciné cameras photographing a shadowgraph image of the flow or the distortions produced in a set of fine parallel lines viewed through the tank. Profiles were made using a single electrode probe to measure conductivity and a hot-film anemometer to measure the horizontal speed of the fluid. The probes were at the same level in the same vertical plane normal to the tube, but $3{\cdot}3\,\mathrm{cm}$ apart on either side of the centre. The output from these probes was recorded on an ultra-violet recorder. On the same record 'event marks' were registered to denote the times at which the tube was tilted and the cameras operated.

The tube was filled in an inclined position, and then slowly tilted into the horizontal. After about 20 min, when the motions had died away, the probes, mounted on 3·2 mm diameter tubes, were traversed vertically through the depth of the fluid at about 10 cm s^{-1} to obtain profiles of conductivity and anemometer output. The output of the conductivity probe and its electronic circuits was linear and closely proportional to the density of the fluid, so that the trace on the recorder was equivalent to a vertical profile of density. The densities in the upper and lower layers were determined with density bottles as the tank was filled, and no further calibration of the density trace was therefore necessary. An example of the density profile ρ_I is shown in figure 14 (*b*). (This will be discussed in detail in § 3.5.) The anemometer record at this stage was used solely to test whether the probe was working properly.

The tube was left to stand in this position until, through molecular diffusion, the interface had broadened to the desired thickness. A final profile was then made and the sensors on the probes left in the fluid, exposed to the subsequent flow about 1 cm below the top of the tank. After a further 3 min to allow the disturbance caused by the probes to disperse, the cameras were started and the tube was suddenly tilted through an angle of about 8°, left for a predetermined time (a few seconds) until the required value of R_I was reached, and then returned again to the horizontal position. Measurements of the flow were then made with the probes. These were of two kinds, either a single vertical profile of density and horizontal velocity from the top to the bottom of the tank at some time τ after the onset of turbulence (see § 3.5), or continuous measurement of the fluctuations at some fixed level in the flow (see § 3.4).

The uniformly accelerating flow when the tank was tilted provided an excellent *in situ* calibration for the stationary anemometer, and it was found to be approximately linear for flow speeds above 3 cm s^{-1}. An *in situ* calibration of the vertically moving anemometer was also achieved. We allowed the motion in the tube to settle after the experiment, and diffusion to remove any remaining fine-scale density structure. The tube was then tilted for the same time as in the experiment, thus [see equation (2)] producing the same flow speed in the homogeneous upper and lower regions as before, and a second vertical profile was made with both probes. The velocity profile (and in particular the gradients at $z = 0$) was then easily calculated from the measured density profile (with Q-correction), and thus the anemometer output, in a vertical profile through an interface of similar dimensions to that of the experiment, was calibrated. This calibration could be made with some confidence, for we know, from earlier experiments in which the flow speed was measured by tracking neutrally buoyant particles (III), that (2) provides an accurate estimate of the observed speeds.

We made estimates of the velocity and density gradients (or equivalently the thicknesses of the interfaces) from the vertical profiles by fitting, by eye, the best straight line through the profiles near $z = 0$. This method is prone to errors. We calculate that the probable worst errors in estimated values in single experiments are 4 % for U_0, 4 % for $\sqrt{\pi/\beta}$, 2 % for Q, 16 % for R_I, 10 % for R_e, 0·5 % for Δ, and 8 % and 15 % for the final mean thickness of the density and velocity profiles respectively. To reduce these errors our results are presented as average values

over several (usually four or five) experiments in the relevant parameter range.

The cameras recorded the overall development of the instability. The still 35 mm camera operated at about 3 frames/s and the times at which photographs were taken were recorded on the ultra-violet recorder. The 16 mm ciné camera, at about 26 frames/s, provided a more complete record, and events sensed by the probes could be related to the appearance of the flow in the photographic record.

3.2. *The growth of the waves*

The initial growth of the waves has not been studied in much detail in these experiments for it is difficult to observe the waves when they are very small, and the presence of permanent probes disrupts the flow. Scotti & Corcos (1972) have however found reasonable agreement between theory and their observations of waves growing in a stratified wind tunnel. At a value of $s = 0{\cdot}064$ we have measured the growth rates (II) and found them to be scattered, but, in the mean, reasonably close to predicted values for infinitesimal waves in the range $0{\cdot}04 < R_I < 0{\cdot}12$. The variation of the non-dimensional wavenumber $k = \pi^{\frac{3}{2}}/(\lambda\beta)$ (where λ is the wavelength) with Q suggested in II has been substantiated in the present set of experiments with mean values of $k = 0{\cdot}40$ and $0{\cdot}34$ at $Q = 0{\cdot}90$ and $0{\cdot}77$ respectively, but with a standard deviation in k of $0{\cdot}05$. This trend in k is in accordance with the predictions of Hazel (1972).

At larger wave slopes, as the waves roll up into billows, the amplitude grows almost linearly with time. Values of da/dt (a is the wave amplitude) vary from about $0{\cdot}12U_0$ at $R_I = 0{\cdot}06$ to about $0{\cdot}05U_0$ at $R_I = 0{\cdot}13$, but with considerable variation from one wave to another (for example, see II, figure 9). The growth rate eventually decreases and the billows appear to reach a limiting amplitude. At almost the same time the first appearance of small-scale structure, or turbulence, is noticed within the billows. Whether the billow amplitude is limited by the onset of turbulence within its spiral structure, or whether by some other kinematic or energy condition, we have not been able to satisfy ourselves. Figure 2 (plates 3 and 4) shows the billows near this state at several values of R_I, and the variation of s (the height-to-wavelength ratio) with R_I is shown in figure 3. The value of s decreases as R_I increases. No significant variation with Δ, Q or R_e has been found.

3.3. *The spread of the region of fine density structure*

In II and III we described how the small-scale structure in the density field, which we associated with turbulence, spreads to fill the billows, and how the billows then elongate in the direction of the flow, amalgamate and spread vertically (see figure 1). The edge of the region of small structure is clearly distinguished when seen against the set of fine lines, and it is a simple matter to measure the mean thickness of the region from the ciné film, by projecting it, one frame at a time, onto a sheet of paper, tracing a line around the edge of the region, and by cutting out and weighing each drawn image. The mean thickness of the fine-structure at the time each frame was taken is then found by comparing the weights with that of a strip of the same length and of height one centimetre on the

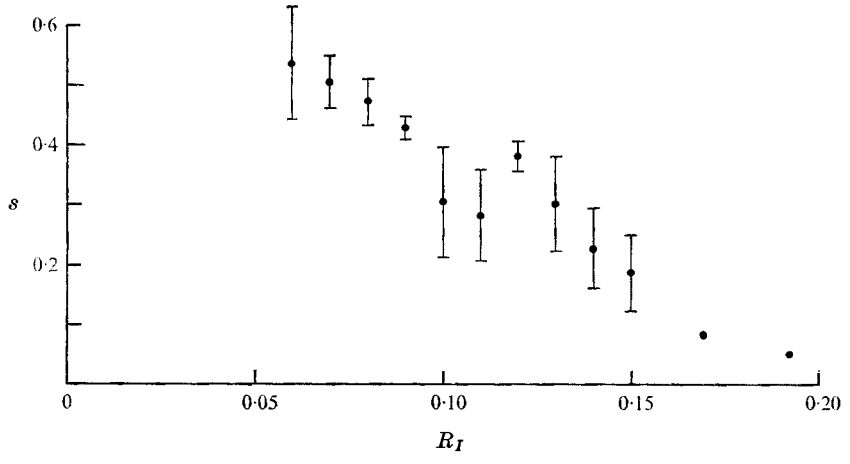

FIGURE 3. Graph showing the variation of s with R_I. The vertical lines represent one standard deviation of s on either side of the mean.

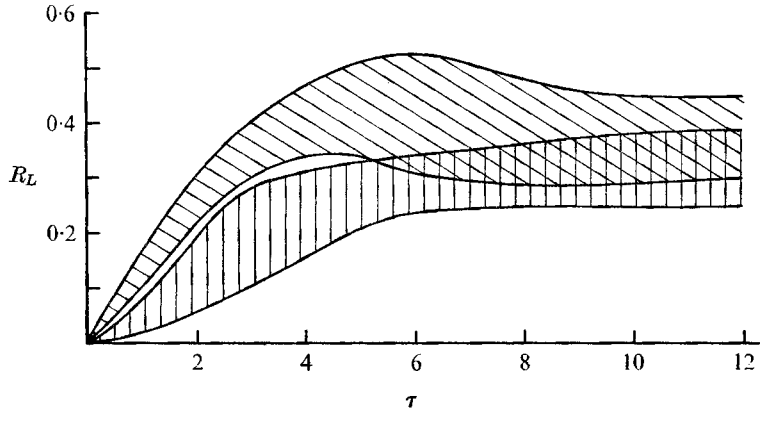

FIGURE 4. The variation of the mean width R_L of the region of fine-structure, with time τ. The vertically hatched region shows the total range for values of R_I close to 0·14 and the diagonally hatched region is for values of R_I close to 0·10.

scale of the projected image. We have plotted the non-dimensional height $R_L = g\Delta T/2U_0^2$ (where T is the thickness of the region) against τ (the non-dimensional time from the onset of fine-structure), and the scatter in the measured values at two values of R_I is shown in figure 4. No significant variations with Q, Δ or R_e have been noticed, and the dominant parameter, in the range of the experimental parameters used, appears to be R_I. For values of R_I between 0·05 and 0·10, R_L grows initially at a rate near $0{\cdot}1\tau$ (so that the boundary of the layer grows at a rate $0{\cdot}1U_0$, like a homogeneous mixing layer), the billows amalgamate to form a continuous layer of turbulence at about $\tau = 2$, and there is a slight 'overshoot' at $\tau = 5$ before the thickness settles, at about $\tau = 7$, to a fairly steady value near 0·4. Small, horizontally elongated regions, in which the lines behind the fluid can again be clearly distinguished, reappear at about $\tau = 12$ between the upper and lower boundaries of the layer. Striations are seen at the same time

in the shadowgraph, indicating a collapse of the vertical mixing processes and the re-establishment of dominant vertical density gradients. At larger values of R_I, the initial growth is less rapid, although rates approaching $0{\cdot}1\tau$ are still found at $\tau = 3$. Billows amalgamate at about $\tau = 2$, as before, but there is no noticeable 'overshoot'. There is little change in the thickness after $\tau = 7$ when R_L is approximately 0·33 and striations appear at about $\tau = 12$, as before.

These observations show that the time scale for the transition process is not strongly dependent on R_I. The main evolution of the layer as controlled by turbulent processes has ended at about $\tau = 12$. We shall see in the following sections how this conclusion is supported by the probe measurements.

3.4. *Measurements at a constant depth*

Figure 5 shows the density and horizontal component of current measured by stationary probes at five different heights in the flow developing from instability in experiments with R_I near to 0·1. The height h above $z = 0$ is non-dimensionalized so that $R_h = g\Delta h/U_0^2$. The tank boundaries were at about $R_h = 4{\cdot}5$. The depths of the two layers were equal and (see II) the waves were stationary. The velocity scale in figure 5 differs from one experiment to another, and the traces from some of the experiments do not begin at $\tau = 0$ (when fine-structure is first observed), for, to avoid unnecessary disturbance, the probes were not lowered into their stationary position until the waves were seen. The traces show large, high-frequency fluctuations during the early stages, but these decay in amplitude and frequency as τ increases. There is evidence of relatively-high-frequency fluctuations persisting in the density trace after they have largely disappeared from the velocity.

The delay in the appearance of any change in density at $R_h = 0{\cdot}06$ (figure 5*a*) until $\tau = 1{\cdot}7$ is due to the probe being positioned between neighbouring billows. Figure 6 (*a*) (plate 5) is a photograph at $\tau = 1{\cdot}5$. The probes have increased the local disturbance; however by $\tau = 11{\cdot}3$ (figure 6*b*, plate 5) there is little remaining evidence of this local disturbance and at $\tau = 18{\cdot}9$ (figure 6*c*, plate 5) the reappearance of lines in the central regions indicates the collapse of vertical motions. Figure 5 (*b*) shows the decaying fluctuations at $R_h = 0{\cdot}17$. The time for an eddy of length λ, convected at speed U_0, to pass a fixed point is λ/U_0, or $g\Delta\lambda/U_0^2$ on the non-dimensional time scale. This is 0·6 in this experiment. A convection speed $\frac{1}{2}U_0$ is probably more realistic at the level of the probe and a time scale 1·2 corresponds approximately to the period of the large fluctuations seen in the trace. Figure 7 (plate 6) shows the appearance of the flow at $\tau = 4{\cdot}7$ and $\tau = 12{\cdot}0$. The onset of fluctuations at $R_h = 0{\cdot}23$ (figure 5*c*) is delayed because the probe was between and slightly above the level of two neighbouring billows. (Billows were frequently found to grow in positions on either side of the probes, and it seems likely that this was due to the slight disturbance caused by the probes even though they projected only a centimetre or so into the tank.) Figure 8 (plate 7) shows the appearance of the flow at $\tau = 4{\cdot}9$ and 10·3. The persistence of the fine-scale density structure at this level and at $R_h = 0{\cdot}36$ (figure 5*d*) is particularly noticeable both in the traces and in the photographs. Figure 9 (plate 8) shows the flow with the probe at $R_h = 0{\cdot}36$ at $\tau = 0{\cdot}4$, 7·6 and

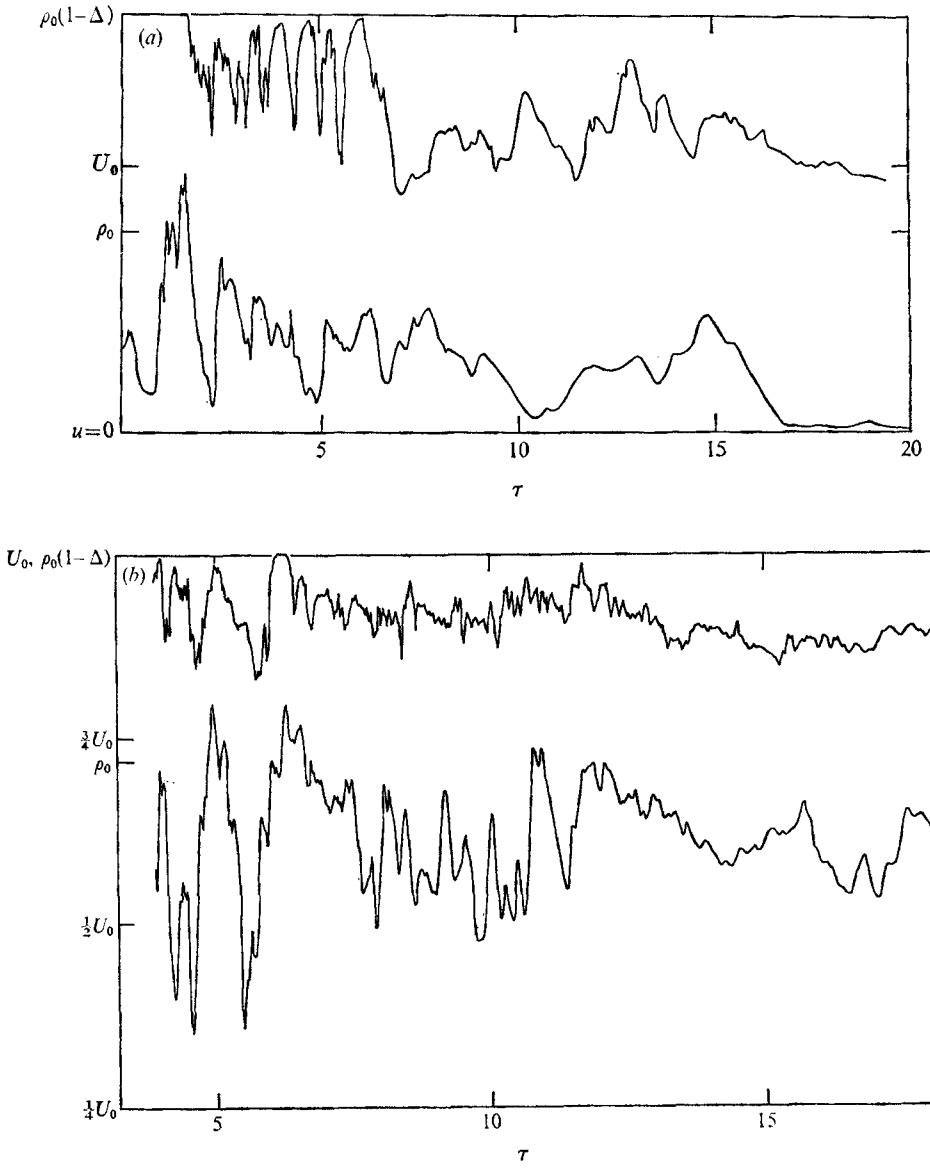

FIGURES 5 (a, b). For legend see facing page.

13·4. The velocity trace is disturbed well before the density is affected. At $\tau = 7{\cdot}6$ a raised region of fine-structure has just cleared the probe, and the associated density and velocity fluctuations can clearly be seen on the traces. The recovery of horizontal structure is shown at $\tau = 13{\cdot}4$. The final trace at $R_h = 0{\cdot}80$ (figure 5 e) shows only a brief, small-amplitude burst in density fluctuations, although the velocity is disturbed soon after the onset of turbulence in the central region. Figure 1 shows the appearance of the flow at various times, and the surge can be seen approaching from the left at $\tau = 19{\cdot}7$.

The onset of high-frequency density structure is generally reflected in a

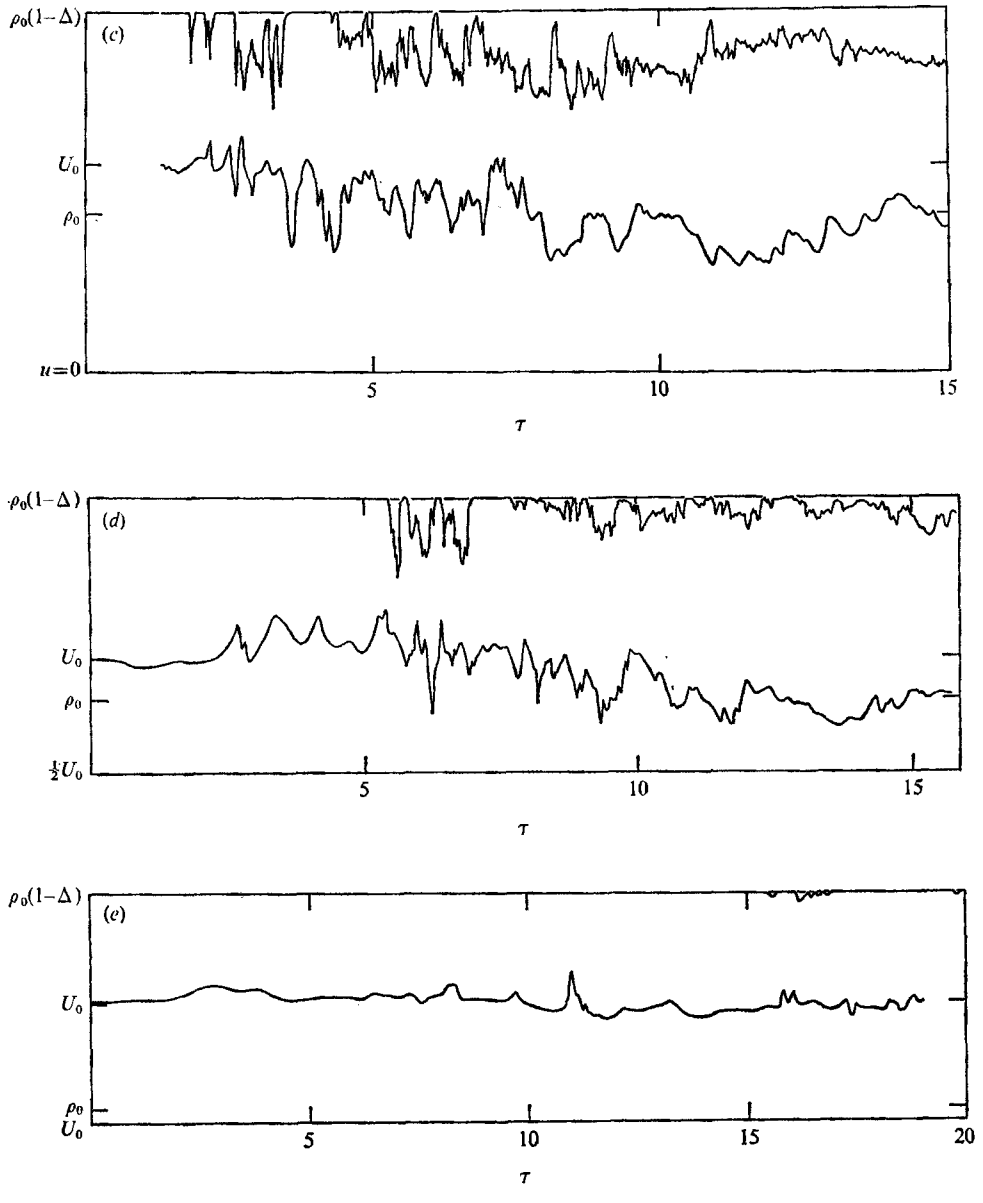

FIGURE 5. The variation of density (above) and total horizontal velocity (below) with time τ at various heights R_h above the centre of the layer.

	R_h	R_I	$\Delta \times 10^2$	Q	R_e
(*a*)	0·06	0·122	2·36	0·83	2210
(*b*)	0·17	0·075	2·06	0·82	3100
(*c*)	0·23	0·084	1·88	0·83	3500
(*d*)	0·36	0·088	1·96	0·83	3260
(*e*)	0·80	0·127	1·91	0·84	2430

response in velocity. There is some correlation between the low-frequency signals at the two probes (at 3·3 cm apart) particularly in the early stages of turbulence, and evidence (especially at $R_h = 0{\cdot}36$ and 0·80) that an irregular motion exists outside the region of influence of the density fluctuations.

It was difficult within the existing apparatus to make horizontal profiles through stationary billows, and so an alternative was adopted: we made the billows move past fixed sensors. This was easily achieved by filling the tube with layers of unequal depths, d_1 above and d_2 below. The speed of the flow in the layers is then $u_1 = 2U_0 d_2/(d_1+d_2)$ and $u_2 = -2d_1 U_0/(d_1+d_2)$ respectively, provided $\Delta \ll 1$ (see I, equation (7)), and the billows move at a speed

$$u_B = \tfrac{1}{2}(u_1+u_2) = U_0(d_2-d_1)/(d_1+d_2).$$

A satisfactory arrangement was obtained by having $d_1 = \frac{1}{3}d_2$, and lowering the probes into the measuring position as the tube was being tilted back into the horizontal after setting up the flow. As in other experiments in which h was very small some disturbance was caused in the lee of the probes, and some effect was probably advected in the lower layer to affect the billows approaching the probe. In the case of small billows (figure 10) at a large value of R_I and low R_e (this was the lowest in all the experiments), the effect was very large in the lee of the probes as is shown in figure 11 (plate 9; the probe Reynolds number was 390), but there was no evidence that the billows were seriously affected before reaching the probes. The probe was slightly above the inflexion point in the initial density profile. The time origin in figure 10 has been arbitrarily positioned, as it was impossible to distinguish fine-structure in the oncoming billows, although there was a lot in the wake. The scale t_λ shown in the figure indicates the time taken for waves of the observed wavelength in the photographs to pass the probe at the calculated speed u_B, and it corresponds very well to the periodicity seen in the traces.

Figure 12 shows traces through moving billows at $R_I = 0{\cdot}10$. The time t_λ for the billows to pass the probe is not short compared with the time taken for the growth of the turbulent layer. The large and sudden changes in density and velocity at $\tau = 0{\cdot}5$ were caused by the passing of an interface between adjacent billows, and figure 13 (plate 10) shows the appearance of the flow at $\tau = 0$, 1·0 and 2·0. The onset of high-frequency fluctuations coincides with the entry of the probe into a billow region of fine-structure, confirming our suspicion that this region is indeed one of rapid velocity fluctuations of a turbulent nature. A correlation is seen in the early part of the record ($\tau < 7{\cdot}5$) between large densities and high horizontal speeds on a time scale of about t_λ, suggesting the advection of semi-coherent structures resulting from the billows. The correlation is consistent with large forward (that is, in the direction fluid above the billows) motion in the upper part of the billows where the density, advected from below in the spiral structure, is greater than outside the billows at the same level. There appears to be little correlation on time scales much less than t_λ.

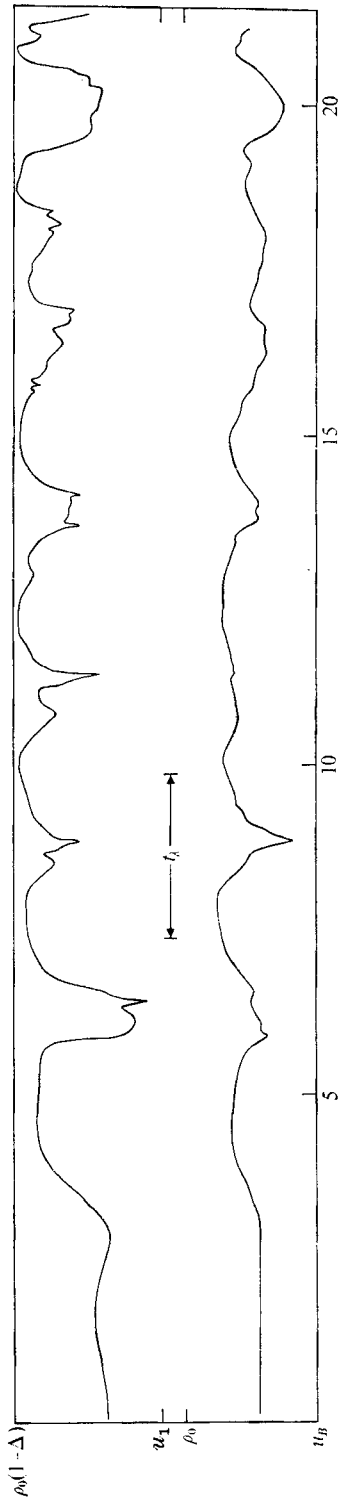

FIGURE 10. The variation of density and total horizontal velocity with time τ through weak billows moving with speed u_B at $R_I = 0{\cdot}178$, $Q = 0{\cdot}85$, $\Delta = 1{\cdot}71 \times 10^{-2}$, $R_e = 1430$. The zero on the τ axis has been positioned arbitrarily.

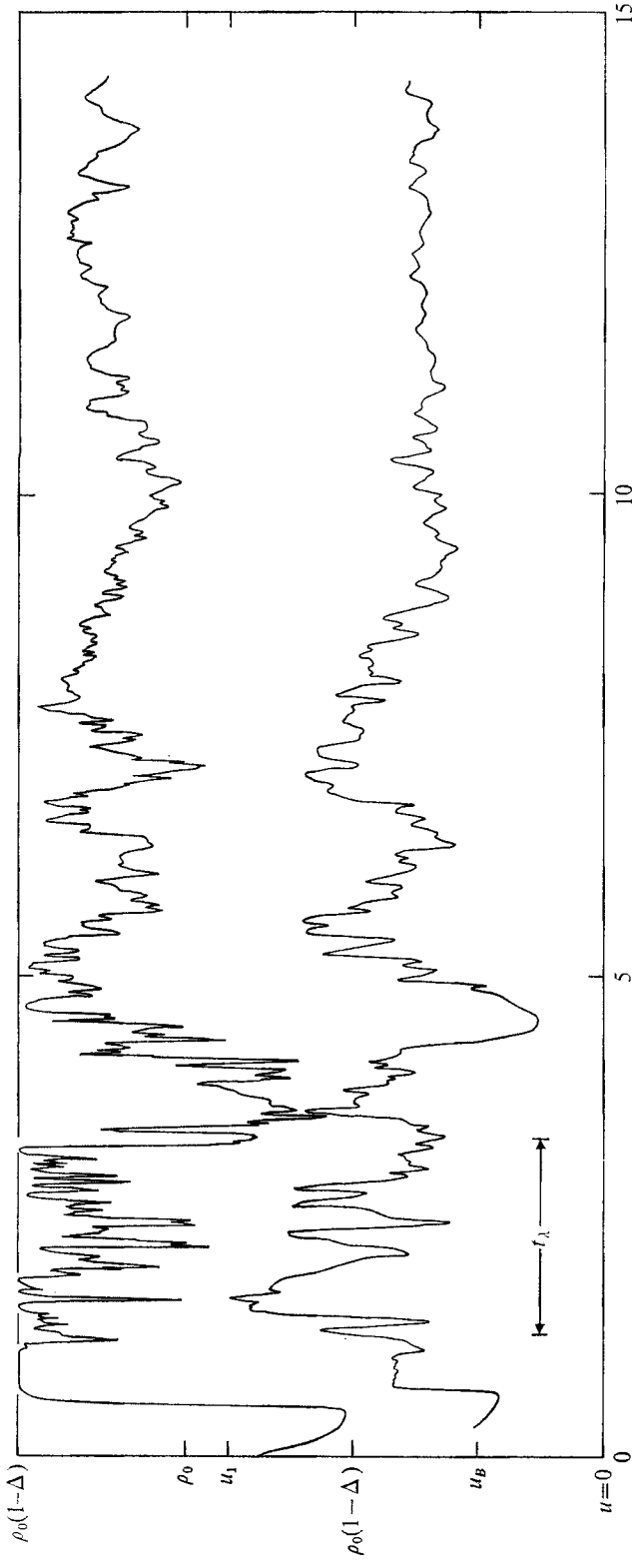

FIGURE 12. The variation of density and total horizontal velocity with time τ through billows moving with speed u_B at $R_I = 0{\cdot}10$, $Q = 0{\cdot}84$, $\Delta = 1{\cdot}90 \times 10^{-2}$, $R_e = 2900$.

3.5. *Vertical profiles*

Some vertical profiles of density made at different times τ for R_I, Q, Δ and R_e approximately equal to 0·070, 0·80, $4{\cdot}4 \times 10^{-2}$ and 2700 respectively, and equal layer depths, have been published already in III. Vertical profiles of both density and horizontal velocity at $\tau = 5{\cdot}7$ and 16·1 are shown in figure 14, and figure 15 (plate 11) shows the appearance of the flow as the profiles were being made. The profiles which immediately follow the onset of turbulence are very irregular and contain parts which are gravitationally unstable. The mean (horizontally averaged) profiles at these times are not known, and the actual profile which is obtained depends very much upon its precise position, for example, whether it is through the centre or edge of a spreading billow. At later times when the photographs show a greater degree of horizontal uniformity, the profiles are less variable, and have nearly uniform gradient in the central regions with mean gradients gradually decreasing to zero in the outer regions. The profiles approximate to error-function profiles although the gradients are slightly more uniform near the centre. Superimposed on the mean are small-scale irregularities which are more persistent near the edge of the layer than near the centre.

We have examined the thicknesses of the density and horizontal velocity interfaces (l_ρ and l_u respectively are the half-thicknesses) and their variation with R_I for $\tau > 12$. The ratio l_u/l_ρ increases as R_I increases above 0·10, and does not appear to be strongly dependent on Δ, Q or R_e, having values $l_u/l_\rho = 1{\cdot}11$, 1·13, 1·12, 1·21 and 1·39 (with a mean variation† of $\pm$ 0·17) at $R_I = 0{\cdot}06$, 0·08, 0·10, 0·12 and 0·14 respectively. The ratio varies, however, in such a way as to keep the final gradient Richardson number $R_F = g\Delta l_u^2/(U_0^2 l_\rho)$ at the centre of the layer almost constant and equal to $0{\cdot}322 \pm 0{\cdot}063$ (error is one standard deviation; 15 observations), having no noticeable trend with Δ, Q or R_e. In these estimates we have only accepted those experiments in which the mean profiles are not significantly influenced by viscosity by using a criterion which we shall discuss in the next section.

4. Discussion

In a general stratified flow it is necessary to know the precise distributions of velocity and density in order to calculate the minimum gradient Richardson number at which infinitesimal waves first grow, or the growth rate or wavelength of the most unstable wave (see, for example, Hazel 1972). It seems probable however that, when the amplitude of the waves becomes large and the fluid near the interface is redistributed in the billow structure, the flow characteristics become less dependent on the exact distributions of velocity and density in the initial flow, provided that the flow contained a single interface at which there was a transition in speed and density, and tended to uniform conditions far above and below the interface. This idea is supported by the observations that, for example, s, the maximum billow height-to-wavelength ratio, is not dependent on Q whereas

† The mean variation is equal to half the average of the differences between the largest and smallest individual measurements made in $(R_I - 0{\cdot}01,\ R_I + 0{\cdot}01)$ for each R_I.

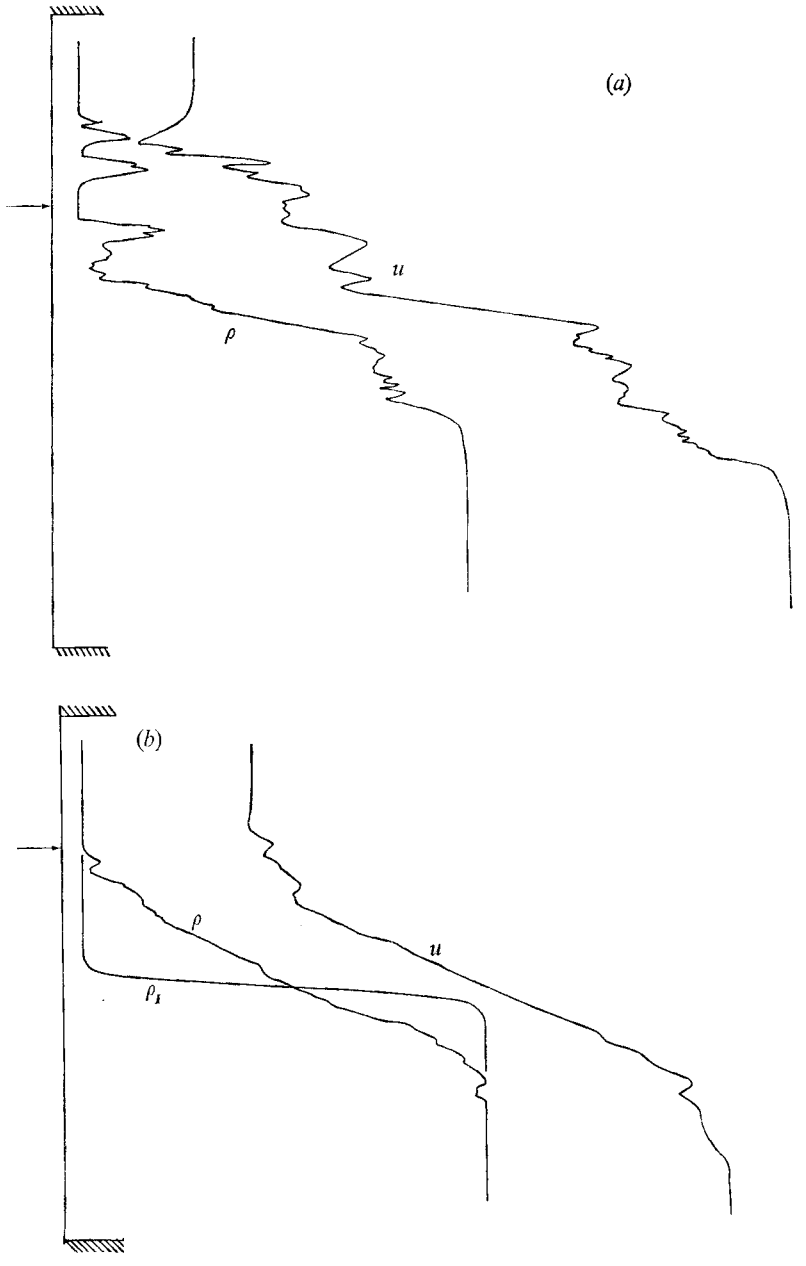

FIGURE 14. Vertical profiles of density and total horizontal velocity. (*a*) $R_I = 0{\cdot}092$, $Q = 0{\cdot}83$, $\Delta = 2{\cdot}29 \times 10^{-2}$, $R_e = 3020$. The downward profile was begun at $\tau = 4{\cdot}2$ and ended at $\tau = 7{\cdot}2$. (*b*) $R_I = 0{\cdot}072$, $Q = 0{\cdot}80$, $\Delta = 2{\cdot}64 \times 10^{-2}$, $R_e = 2490$. The downward profile was begun at $\tau = 14{\cdot}7$ and ended at $\tau = 17{\cdot}6$. The profile of density before the onset of instability is also shown and is marked ρ_I. The hatched lines show the position of the boundaries of the tube and the arrows on the right show the position of the probe at the times when the photographs of figure 15 were taken.

k, the non-dimensional wavenumber, is. The variation found in s with R_I, as well as the observations of the eventual structure of the turbulent layer at large τ, may apply to a wider range of initial density and velocity profiles rather than to error-function profiles alone, common as these may be in natural phenomena. Whilst we need to have a better understanding of the controlling dynamics of the flow before this conclusion can be justified, it is tempting to examine the range of values of s found by Browning (1971) in atmospheric billows and to infer from figure 3 the possible range of values of R_I at which the billows developed, and from §3.5, the change in the velocity and density structure which may have accompanied their decay. The exercise is left to those readers who succumb to the temptation. They should be warned that there is a problem of extrapolating the laboratory data. The major differences between the atmospheric billows, for example those observed by Browning, and those in the laboratory are in the appropriate Reynolds numbers of the flow and the Rayleigh numbers in the overturning billows. (Estimates of these values are given in III.) The size of these parameters makes it probable that turbulence becomes fully developed in the atmospheric billows, whilst it is not fully developed in the laboratory. Evidence for the existence of small scales of motion in the atmospheric billows can be found in the aircraft and balloon measurements. Temperature fluctuations on a scale minute compared with that of the billows produce the radar backscatter by which the structures are detected. The consequence of this intense turbulent mixing may be to produce a better-mixed layer than we find in the laboratory. The parameters in the ocean thermocline do not, however, differ greatly from those in the laboratory, and a similarity of structures and their development is likely.† We return to this point later. The fairly long time taken for probes to pass through

† In naturally occurring phenomena, single vertical profiles of both velocity and density are always very irregular, containing fluctuations on scales down to a viscous, or diffusive, cut-off. Horizontal and temporal variations are also present. The minimum Richardson number measured from a single vertical profile containing such fine-structure can have little relevance to the subsequent evolution of billows which have scales many times greater than the scale on which the Richardson number varies significantly. In the atmosphere all that is available is often the information from one, or perhaps two, radiosonde ascents. The question arises: can an appropriate Richardson number be ascertained? This is a question which deserves full investigation. It is likely however that, since the observed billows have a notable spatial uniformity, horizontal fluctuations of the appropriate R_I are not significant over a few billow wavelengths. A coherence between vertical and horizontal structures is often found in the ocean thermocline, a given vertical structure having coherence over a horizontal scale 50–500 times its vertical scale, except at the very smallest scales (less than the Ozmidov scale; see Ozmidov 1965), where motion may be isotropic. The ratio of scales appears to increase as the scales themselves increase, but it is possibly bounded by a number of order N/f, where N is a mean Brunt–Väisälä frequency horizontally averaged over the vertical scale in question, and f is the Coriolis parameter. The Brunt–Väisälä frequencies in the atmosphere and the ocean have similar values. If the atmosphere has similar coherence properties at the level in which billows are found, then the thickness of structures which are coherent over several billow wavelengths can be calculated. The appropriate Richardson number might be found from the vertical profiles after filtering out structures which have a smaller vertical scale. It appears that the resolution which is usually obtained from radio-sondes (about 100 m) may not be sufficiently small for the record to distinguish the vertical structures which are coherent over several of the shortest (800 m) wavelength billows described by Browning (1971).

the moving billows (§3.4) makes the records rather different from profiles obtained by the relatively rapid traverses which have been made through atmospheric billows, but similarities are evident when the records are compared, particularly the large gradients at the tilted interfaces between billows.

The fluctuations in the density and horizontal velocity, and the development of the turbulent layer, have been discussed in §3. The probe measurements augment the visual observations and lend support to the conclusion that the collapse of turbulence occurs near $\tau = 12$. This value also seems to give a reasonable estimate of the persistence time of turbulence following instability in the atmosphere and ocean (see III). The dimensional time for collapse is $12U_0/g\Delta$ or $12/(NR_I^{\frac{1}{2}})$, where N is the Brunt–Väisälä frequency at the centre of the initial interface. The observed persistence of density microstructure ('fossil turbulence') after the decay of velocity fluctuations has also been found in the ocean (see for example Turner 1973, figure 10.2). The lack of coherence between density and velocity fluctuations in the centre of the layer at $\tau > 12$ is explained by the fact that, although internal waves are seen in the ciné films of the flow, the density signal is responding to the presence of the almost horizontal density microstructure, and is 'contaminated' in the same way as signals are by fine-structure in the ocean (Garrett & Munk 1971). Fluctuations in velocity outside the region of density fluctuations have been observed, but these experiments have not established whether the flow in this region is rotational or turbulent, or whether the fluctuations correspond to a potential flow similar, for example, to that outside a turbulent jet in a homogeneous fluid.

Perhaps the most important result of these experiments has been the definition of the form of the mean profiles of density and horizontal velocity when τ is large. Some contribution to the fluctuations in the anemometer records comes from transverse velocities in the tube, and we cannot distinguish between longitudinal and lateral fluctuations. The mean (time-averaged) motion at large τ does, however, appear to be uniform in x, that is, parallel to the tube walls along the tank. We have found no evidence of local circulations or helical motions when the motion of neutrally buoyant beads are observed. The mean profiles at large values of τ can be approximated by error functions:

$$\rho = \rho_0\{1 - \Delta \operatorname{erf}[z\sqrt{\pi}/(2l_\rho)]\} \tag{6}$$

and

$$u = U_0 \operatorname{erf}[z\sqrt{\pi}/(2l_u)]. \tag{7}$$

The instability can be regarded as a diffusion process in which the profiles given by (1) and (3) (with a correction for viscosity) are changed to (6) and (7), respectively, in a time t_1 (greater than $12U_0/g\Delta$). If the diffusion coefficients required to achieve this change are κ_ρ and κ_u ('eddy diffusion coefficients' for solute and momentum respectively) then

$$\frac{\kappa_\rho}{\kappa} = \frac{4l_\rho^2 - \pi/\beta^2}{4\pi\kappa t_1}, \quad \frac{\kappa_u}{\nu} = \frac{4l_u^2 - \pi/\beta^2 Q^2}{4\pi\nu t_1}. \tag{8}$$

In the experiments the values of κ_ρ/κ ranged from about 2×10^4 at the smaller values of R_I to unity (no significant change in the density profile could be detected) at R_I near 0·19. The largest values of K_u/ν were about 45, and the

smallest close to unity at the larger R_I or smallest values of R_e. Small values of κ_u/ν imply that the effect of molecular viscosity on a parallel flow is as important as any enhanced diffusion caused by the instability, and experiments in which κ_u/ν was less than 4 were not taken into account in the calculation of R_F or in the following analysis.

A quantity which has been subject to considerable investigation in turbulent boundary-layer flow is the ratio κ_ρ/κ_u of the eddy diffusion coefficients, and this is known to decrease as the Richardson number increases (see for example Turner 1973, chapter 5). In these experiments we find $\kappa_\rho/\kappa_u = 0{\cdot}92$, $0{\cdot}83$, $0{\cdot}59$, $0{\cdot}55$ and $0{\cdot}33$, with a mean variation of $0{\cdot}16$, at $R_I = 0{\cdot}06$, $0{\cdot}08$, $0{\cdot}10$, $0{\cdot}12$ and $0{\cdot}14$ respectively; Q, Δ and R_e do not appear to be important parameters. In this single mixing event the ratio of the diffusion coefficients decreases with increasing values of the initial gradient Richardson number. This is a consequence of the increasing ratio l_u/l_ρ. It is significant that there is little diffusion of solute at large R_I but an appreciable transfer of momentum. The flow is thus reduced with little modification to the density field.

We consider now the energy transfer which takes place during this mixing event. Kinetic energy is lost from the mean flow whilst potential energy is gained by the mean density field. Kinetic energy is lost by heat generation due to viscous dissipation in the turbulent motion and to the internal wave field remaining in the final flow. The net gain in mean potential energy is due to enhanced molecular diffusion in regions of increased local solute gradients within the fine-structure region. The local gradients are produced as a result of the distortion of the density field by the field of motion, and in this process kinetic energy will be temporally transferred to and from potential energy. The net gain of potential energy in the final mean density field is not, however, available for transfer back into kinetic energy,† as is the case in standing waves, but comes from the internal energy of the solute (just as potential energy is gained through molecular diffusion at a horizontal interface between static layers of different densities). The kinetic energy lost by the mean flow per unit cross-sectional area is

$$\text{K.E.} = (2/\sqrt{\pi})\rho_0 U_0^2[l_u - \sqrt{\pi}/(2Q\beta)], \tag{9}$$

and the potential energy gained by the mean density field per unit cross-sectional area is

$$\text{P.E.} = (2/\pi)g\rho_0\Delta[l_p^2 - \pi/4\beta^2]. \tag{10}$$

The ratio P.E./K.E. represents the amount of work done on the mean buoyancy field compared with that lost by the mean motion during the mixing event. We find that P.E./K.E. $= 0{\cdot}212$, $0{\cdot}205$, $0{\cdot}182$, $0{\cdot}142$ and $0{\cdot}098$, with a mean variation of $0{\cdot}040$, at $R_I = 0{\cdot}06$, $0{\cdot}08$, $0{\cdot}10$, $0{\cdot}12$ and $0{\cdot}14$ respectively. Proportionally more energy is lost by the mean motion than is gained by the buoyancy field as R_I increases. If both K.E. and P.E. are scaled with $\rho_0 U_0^4/g\Delta$, we find that each decreases as R_I increases with mean values K.E.$(g\Delta/\rho_0 U_0^4) = 0{\cdot}226$, $0{\cdot}203$ and $0{\cdot}098$ and P.E.$(g\Delta/\rho_0 U_0^4) = 0{\cdot}049$, $0{\cdot}042$ and $0{\cdot}010$ at $R_I = 0{\cdot}065$, $0{\cdot}094$ and

† Unless the instability has occurred as a local phenomenon, when some potential energy may be transferred into kinetic energy as a mixed patch later spreads horizontally.

0·142 respectively. (The scaling used here is rather arbitrary and it is possible that a scaling involving ν is more appropriate.) The total energy E per unit cross-sectional area which is dissipated in heat or by internal waves is the difference between these values, and in the range $0{\cdot}045 \leqslant R_I \leqslant 0{\cdot}15$ satisfies approximately the relation

$$E = (\rho_0 U_0^4/g\Delta)\,(0{\cdot}25 - R_I),$$

with standard deviation $0{\cdot}025(\rho_0 U_0^4/g\Delta)$. It is not known what fraction of the energy lost is transferred to the internal wave field.

It is remarkable that the final gradient Richardson number R_F in the layer appears to be independent of R_I, and this result merits further study.

The increase in l_u/l_ρ when R_I is sufficiently large (but of course less than the critical value necessary for instability) may be sufficient to allow a second kind of instability to occur. For hyperbolic-tangent profiles of velocity and density, Hazel (1972) has shown that, when the velocity interface has a thickness more than twice that of the density interface, the gradient Richardson number at the edge of the layer is less than that in the centre, and a non-stationary instability can occur at the edge of the region rather than in the centre. It seems likely that this instability accounts for the 'cusped waves' described in I. What its effect may be, whether it can again increase the velocity gradients within the layer through the generation of turbulence in the over- and underlying layers, is not yet known. (It is perhaps worth remarking that the situation is different from the boundary layer near a solid wall, where turbulence inevitably extends the region of vorticity. In this case the boundary, the central layer, is free and vorticity can be concentrated near it.) These effects may be important in the ocean, where layers are found to persist for very long times.

Values of R_I much smaller than the range studied in these experiments may occur naturally at the edges of plumes and thermals or where there is some mechanism for producing very large accelerations (equivalent to large angles of tilt of the tube; possible candidates are lee waves and the noses of density currents). Richardson numbers just below the critical value are likely to be fairly common, although they may not lead to large billows or to much modification of the flow, and it would be very useful to extend experimental studies into this region, and in particular to see whether steady finite-amplitude waves of the kind described by Drazin (1972) can be produced.†

Finally, we remark that large mean gradients have not been observed, in either density or horizontal velocity, near the edges of the layer, even in experiments in which the shear was reduced and reversed as instability occurred, by reversing the tilt of the tube, to simulate the effects of periodic shear produced by internal waves. We are thus unable to account for the multiple layers found in the ocean thermocline by Woods & Wiley (1972) and attributed to the action of Kelvin–Helmholtz instability on an interface. The situation might be very different however if instability occurred in an almost constant density gradient in some region where the velocity gradient was locally increased, and in that case it is

† Drazin's work has been extended by Weissman (1973) and several interesting effects have been investigated theoretically, notably the way in which a patch of marginally unstable waves will spread both laterally and longitudinally in a horizontal plane.

probable that the result might be a relatively-well-mixed region bounded by layers of increased gradient.

It is a pleasure to acknowledge the considerable help which has been given by Mr Alan Hall and Mr Paul Tickner in making these experiments, and their expertise in constructing and operating the probes. I am indebted to the Photographic Department of I.O.S. for reproducing photographs, and to Dr K. A. Browning and Dr J. S. Turner for several helpful comments.

REFERENCES

BROWNING, K. A. 1971 *Quart. J. Roy. Met. Soc.* **97**, 283.

BROWNING, K. A., BRYANT, G. W., STARR, J. R. & AXFORD, D. N. 1973 In press.

BROWNING, K. A., HARROLD, T. W. & STARR, J. R. 1970 *Quart. J. Roy. Met. Soc.* **96**, 40.

CERMAK, J. E. & ARYA, S. P. S. 1970 *Boundary-Layer Met.* **1**, 40.

DRAZIN, P. G. 1972 *J. Fluid Mech.* **42**, 321.

FRANKIGNOUL, C. J. 1972 *Geophys. Fluid Dyn.* **4**, 91.

GARRETT, C. & MUNK, W. 1971 *J. Phys. Oceanogr.* **2**, 225.

GARRETT, C. & MUNK, W. 1972 *Deep-Sea Res.* **19**, 823.

GRANT, H. L., MOILLIET, A. & VOGEL, W. M. 1968 *J. Fluid Mech.* **34**, 443.

GREGG, M. C. & COX, C. S. 1972 *Deep-Sea Res.* **19**, 355.

HAZEL, P. 1972 *J. Fluid Mech.* **51**, 39.

HARDY, K. R., REED, R. J. & MATHER, G. K. 1973 *Quart. J. Roy. Met. Soc.* **99**, 279.

MOORE, M. J. & LONG, R. R. 1971 *J. Fluid Mech.* **49**, 635.

ORLANSKI, I. 1972 *J. Fluid Mech.* **54**, 577.

ORLANSKI, I. & BRYAN, K. 1969 *J. Geophys. Res.* **74**, 6975.

OZMIDOV, R. V. 1965 *Izv. Atm. Ocean Phys.* **1**, 853.

READINGS, C. J., GOLTON, E. & BROWNING, K. A. 1973 *Boundary-Layer Met.* (in press).

ROACH, W. T. 1972 *Clear Air Turbulence.* Watford: Merrow Pub. Co.

SCOTTI, R. S. & CORCOS, G. M. 1972 *J. Fluid Mech.* **52**, 499.

THORPE, S. A. 1968 *J. Fluid Mech.* **32**, 693.

THORPE, S. A. 1971 *J. Fluid Mech.* **46**, 299.

THORPE, S. A. 1973 *Boundary-Layer Met.* **5**, 95.

TURNER, J. S. 1973 *Buoyancy Effects in Fluids.* Cambridge University Press.

WEISSMAN, R. A. 1973 Non-linear wave packets in Kelvin–Helmholtz flow. Ph.D. thesis, Dept. of Geophys. Sci., University of Chicago.

WOODS, J. D. 1968 *J. Fluid Mech.* **32**, 791.

WOODS, J. D. & WILEY, R. L. 1972 *Deep-Sea Res.* **19**, 87.

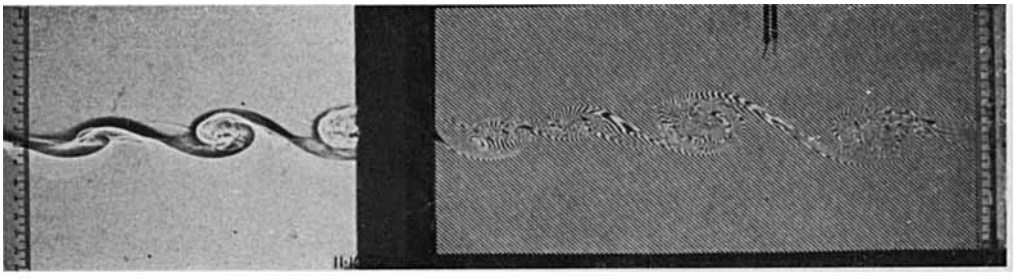

(*a*)

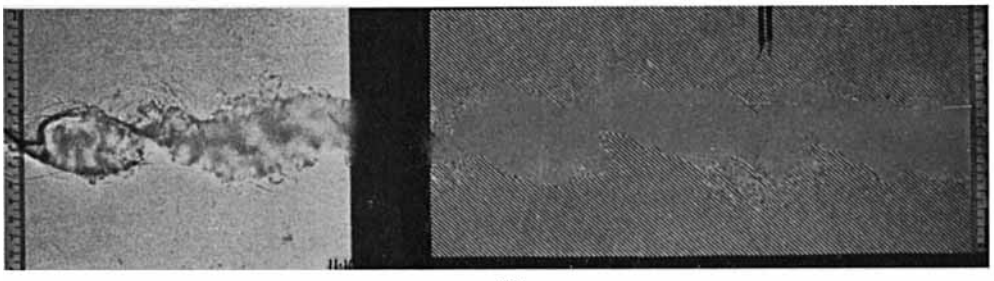

(*b*)

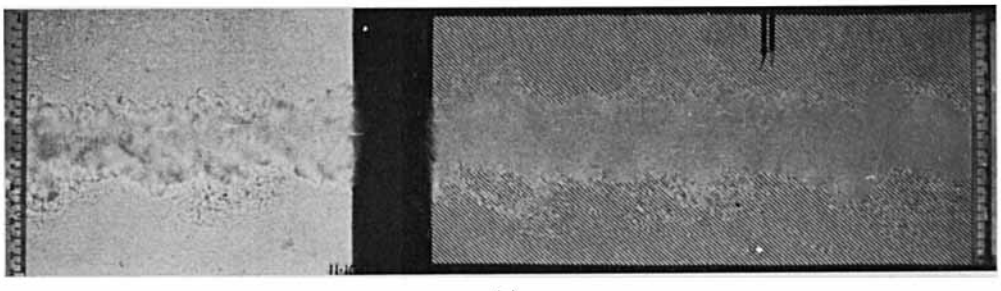

(*c*)

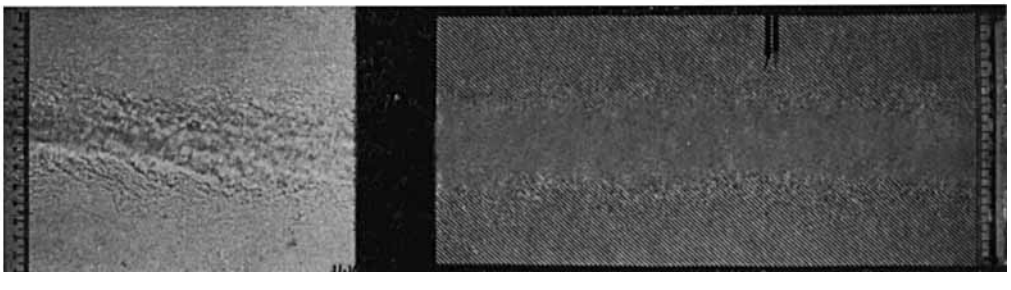

(*d*)

FIGURES 1 (*a–d*). For legend see overleaf.

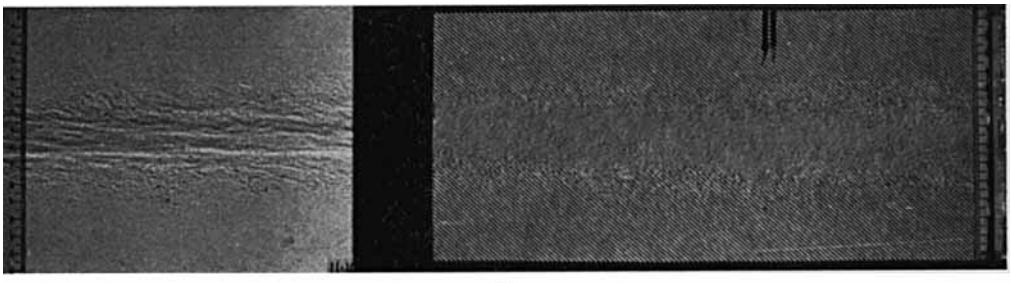

(*e*)

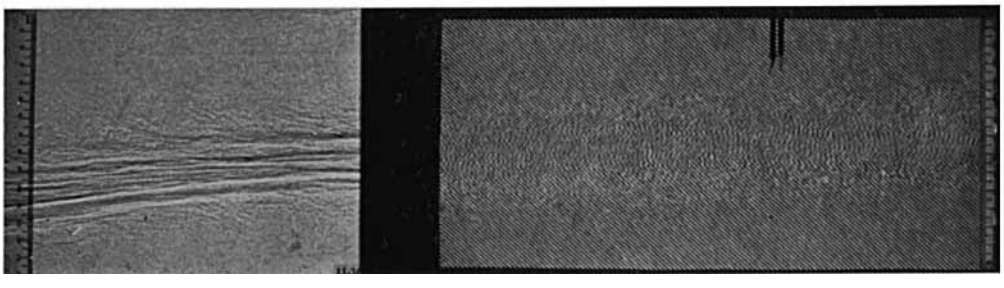

(*f*)

FIGURE 1. Photographs of the appearance of the flow for instability occurring at $R_I = 0{\cdot}127$ for $\Delta = 1{\cdot}91 \times 10^{-2}$, $Q = 0{\cdot}84$, $R_e = 2430$ at the following values of τ: (*a*) 0·4; (*b*) 2·5; (*c*) 4·7; (*d*) 9·7; (*e*) 14·7; (*f*) 19·7. The flow is to the left in the upper layer and to the right in the lower. At the left is a shadowgraph and at the right a set of diagonal parallel lines (approximately 1 mm thick and 1 mm apart) are viewed through the fluid. The probes can be seen silhouetted against the lines, and the record from these probes is shown in figure 5(*e*).

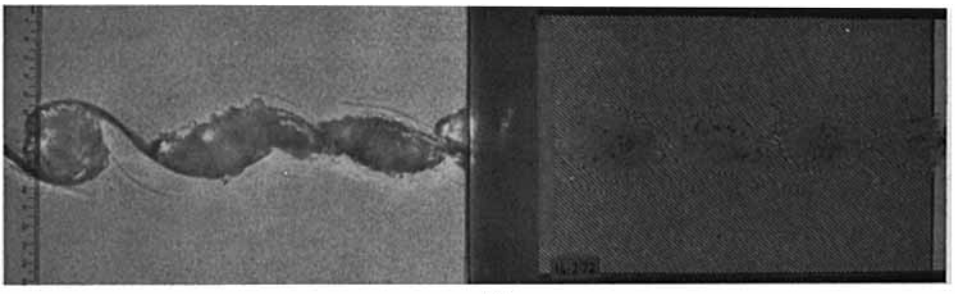

(*a*)

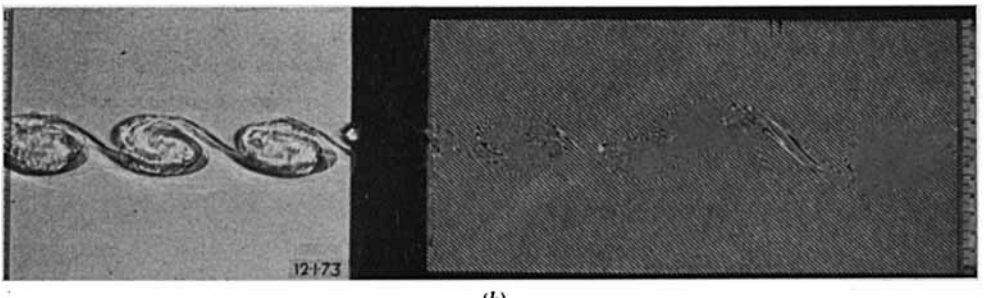

(*b*)

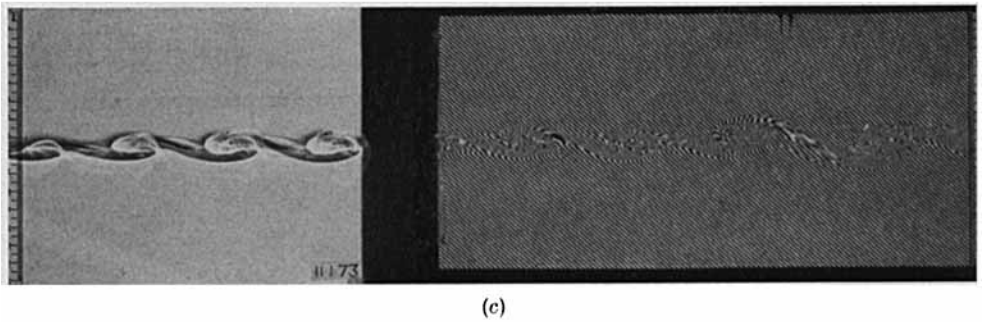

(*c*)

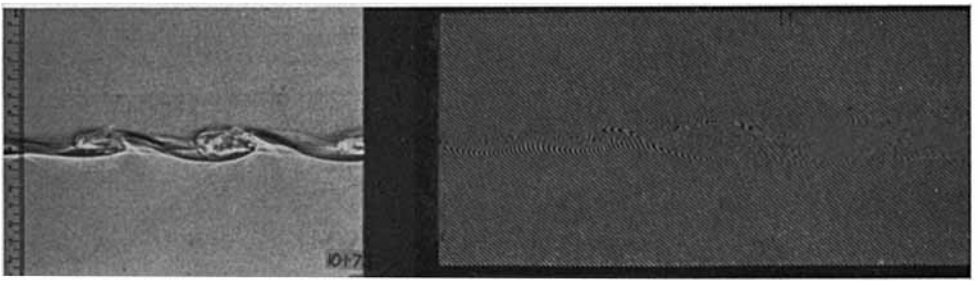

(*d*)

FIGURES 2 (*a*–*d*). For legend see overleaf.

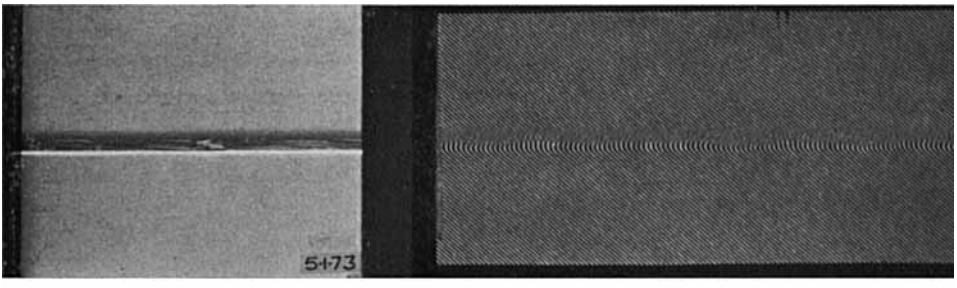

(*e*)

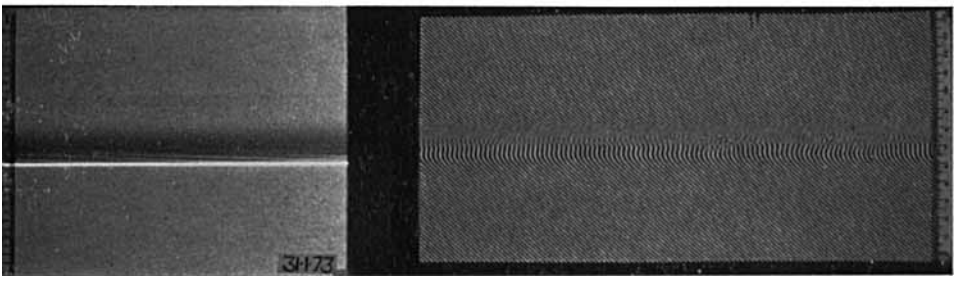

(*f*)

FIGURE 2. Photographs showing the appearance of billows close to the time $\tau = 0$ when fine-structure is first observed,

	R_I	$\Delta \times 10^2$	Q	R_e
(*a*)	0·051	2·96	0·76	2380
(*b*)	0·081	1·96	0·79	2250
(*c*)	0·105	1·97	0·80	1860
(*d*)	0·135	1·97	0·82	1860
(*e*)	0·169	2·00	0·82	1580
(*f*)	0·192	4·88	0·90	4890

The black specks in figure 2 (*a*) are neutrally buoyant particles, which were introduced so that the fluid motions could be followed in the ciné film.

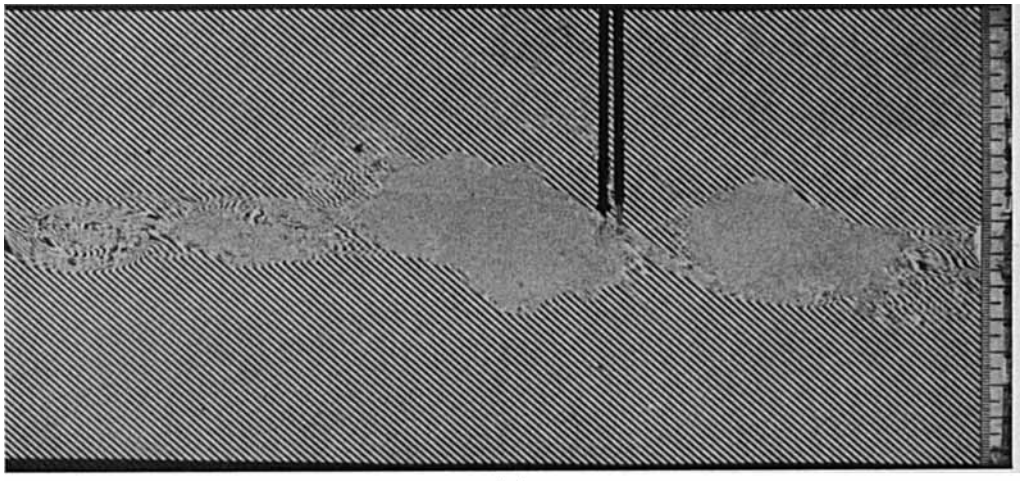

(*a*)

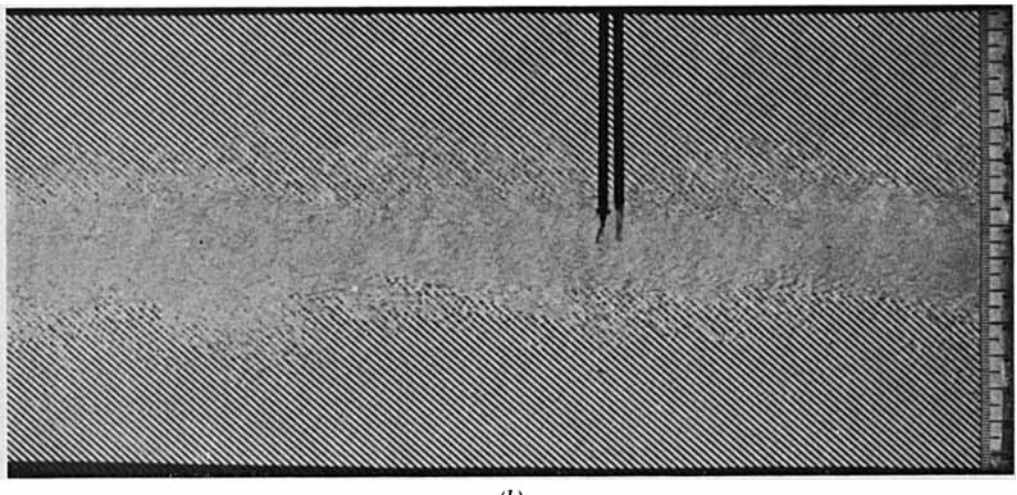

(*b*)

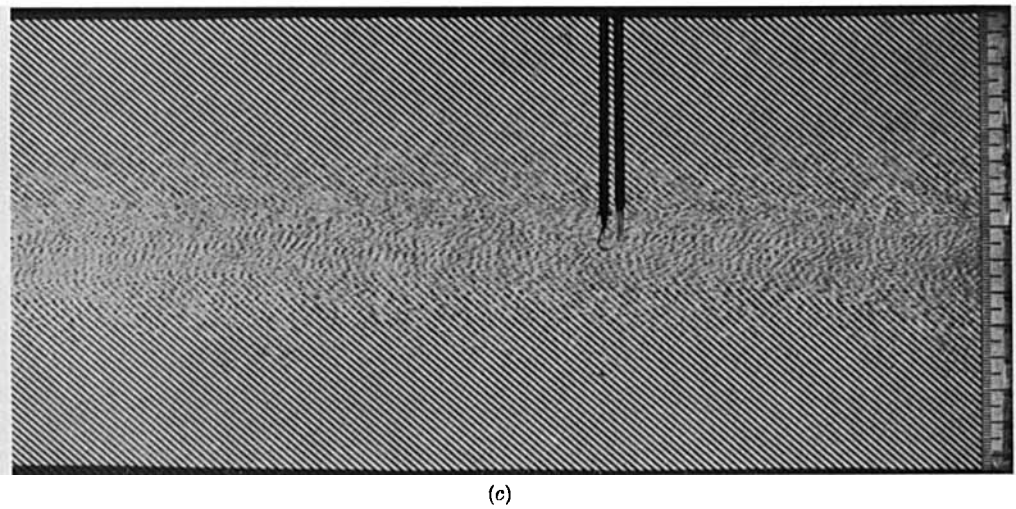

(*c*)

FIGURE 6. Photographs of the flow recorded in figure 5(*a*) at times (*a*) $\tau = 1{\cdot}5$, (*b*) $\tau = 11{\cdot}3$, (*c*) $\tau = 18{\cdot}9$. Flow in the upper layer is to the left.

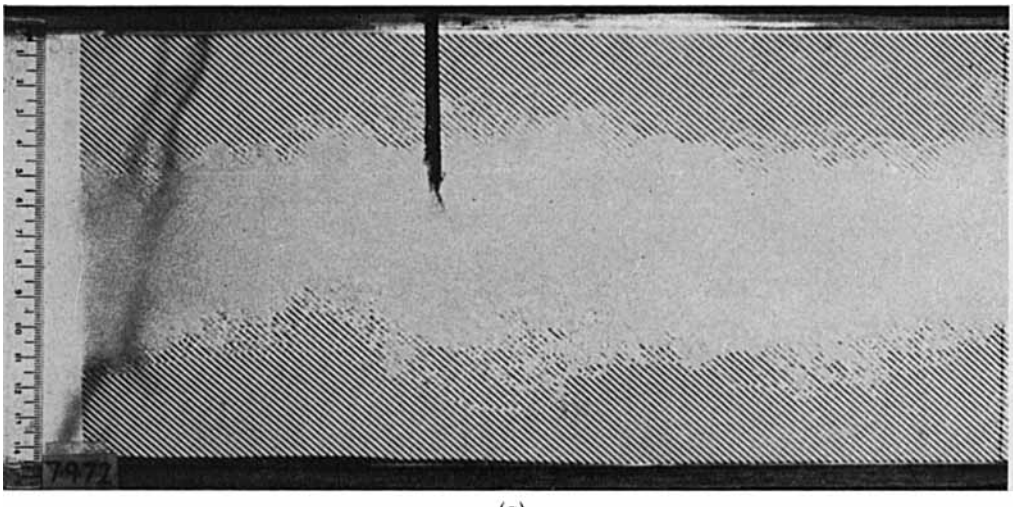

(*a*)

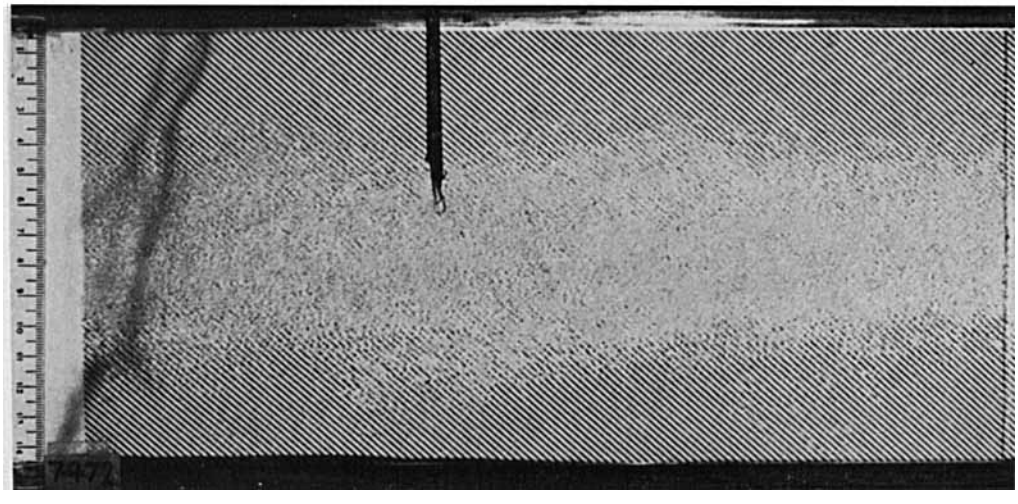

(*b*)

FIGURE 7. Photographs of the flow recorded in figure 5(*b*) at times (*a*) $\tau = 4{\cdot}7$, (*b*) $\tau = 12{\cdot}0$. Flow in the upper layer is to the right.

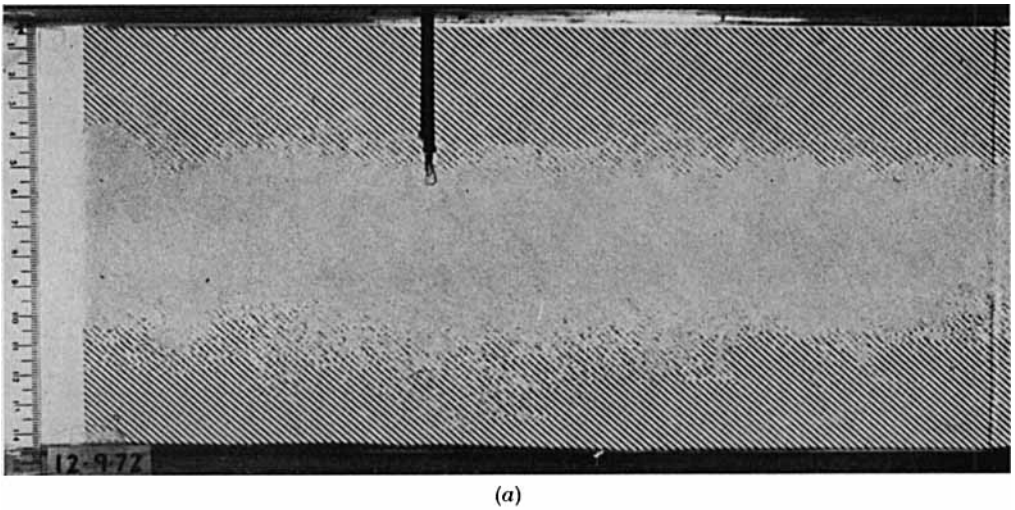

(*a*)

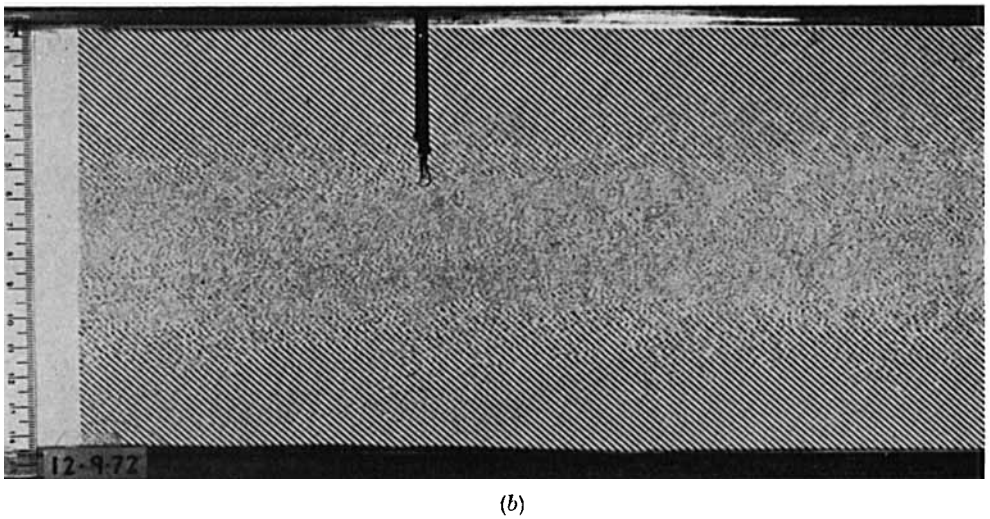

(*b*)

FIGURE 8. Photographs of the flow recorded in figure 5(*c*) at times (*a*) $\tau = 4{\cdot}9$, (*b*) $\tau = 10{\cdot}3$. Flow in upper layer is to the right.

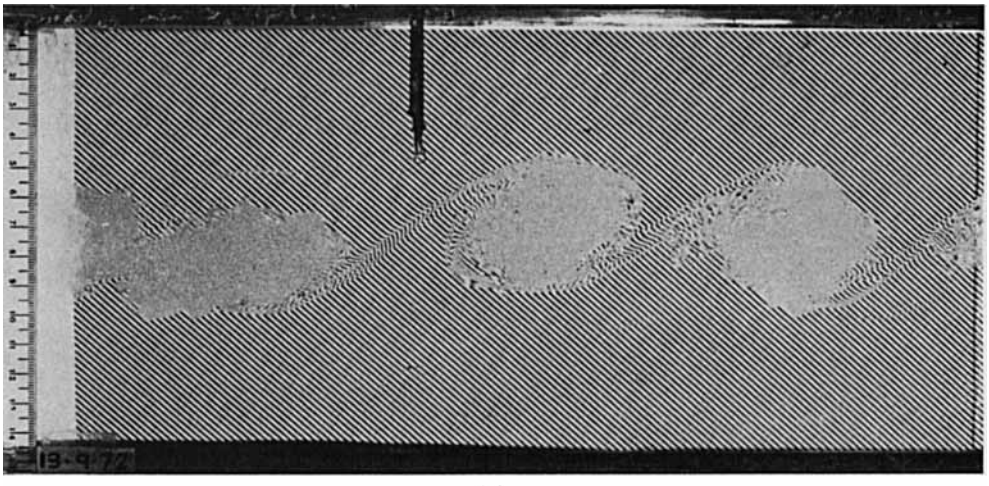

(*a*)

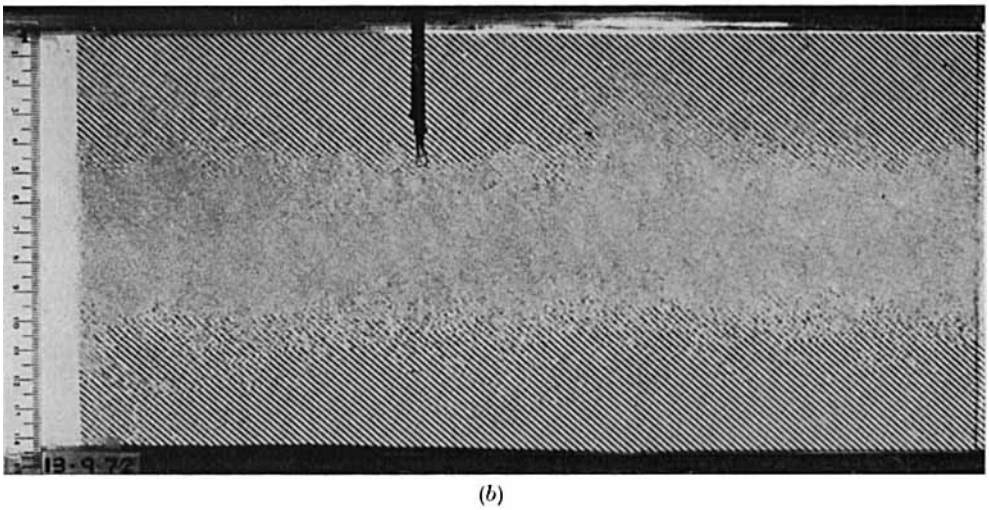

(*b*)

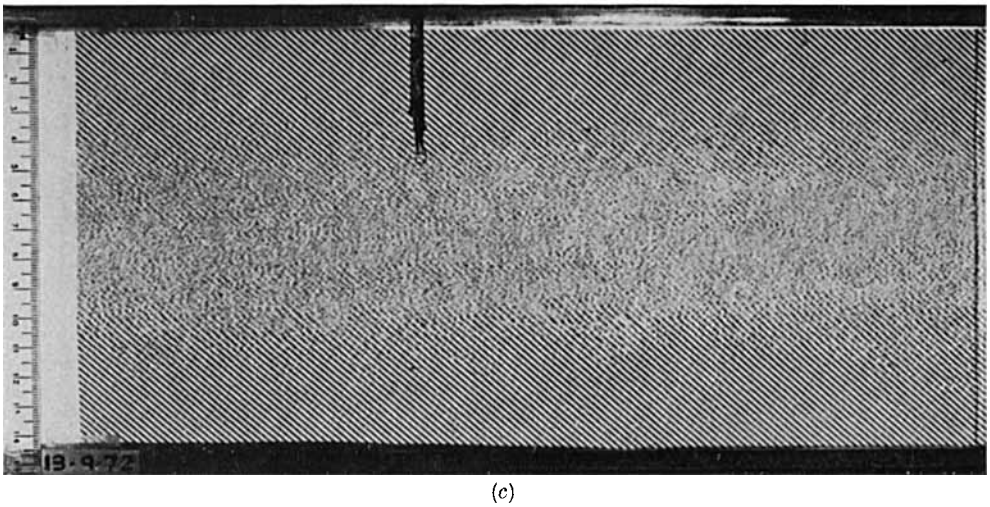

(*c*)

FIGURE 9. Photographs of the flow recorded at figure 5(*d*) at times (*a*) $\tau = 0{\cdot}4$, (*b*) $\tau = 7{\cdot}6$, (*c*) $\tau = 13{\cdot}4$. Flow in the upper layer is to the right.

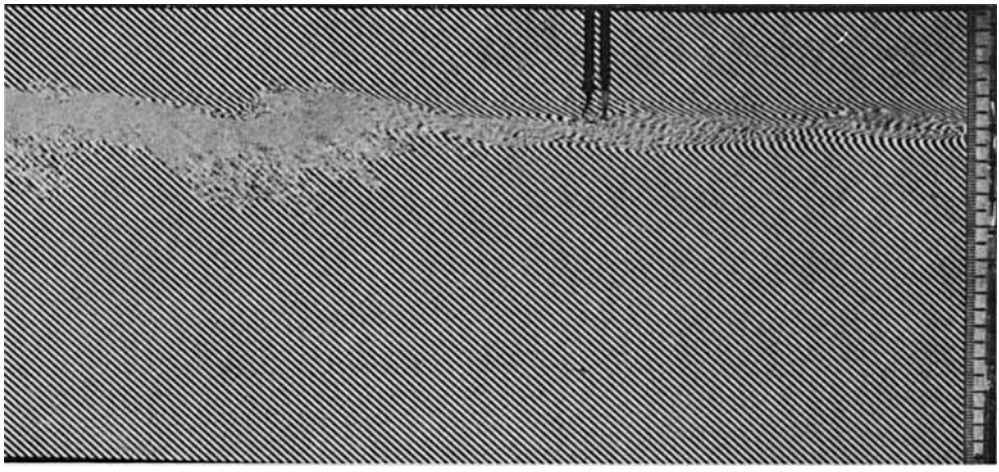

FIGURE 11. Photograph of the flow recorded in figure 10 at $\tau = 8{\cdot}8$. The flow in the upper layer and direction of propagation of the billows are to the left.

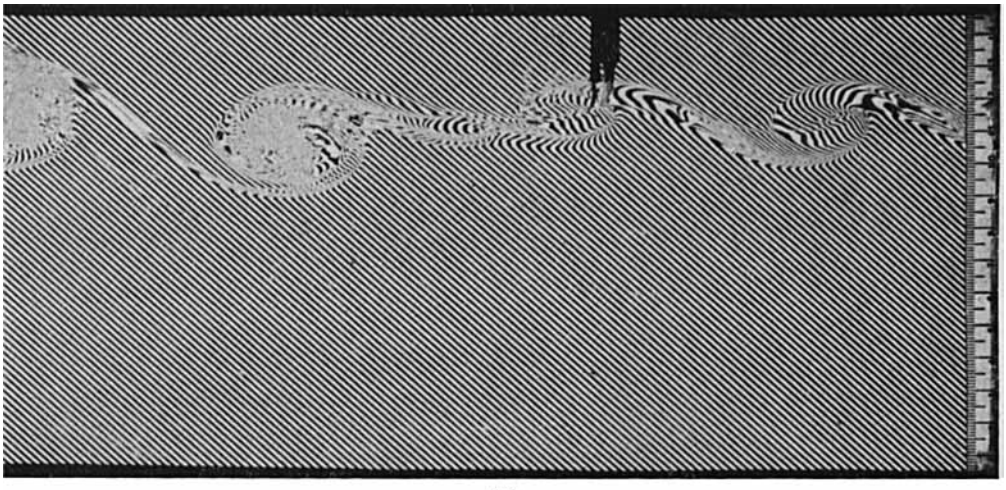

(*a*)

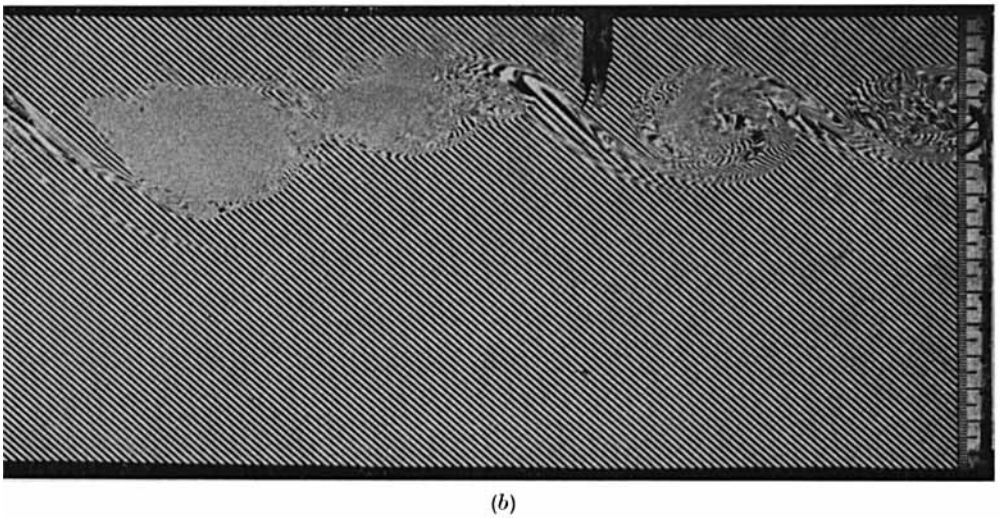

(*b*)

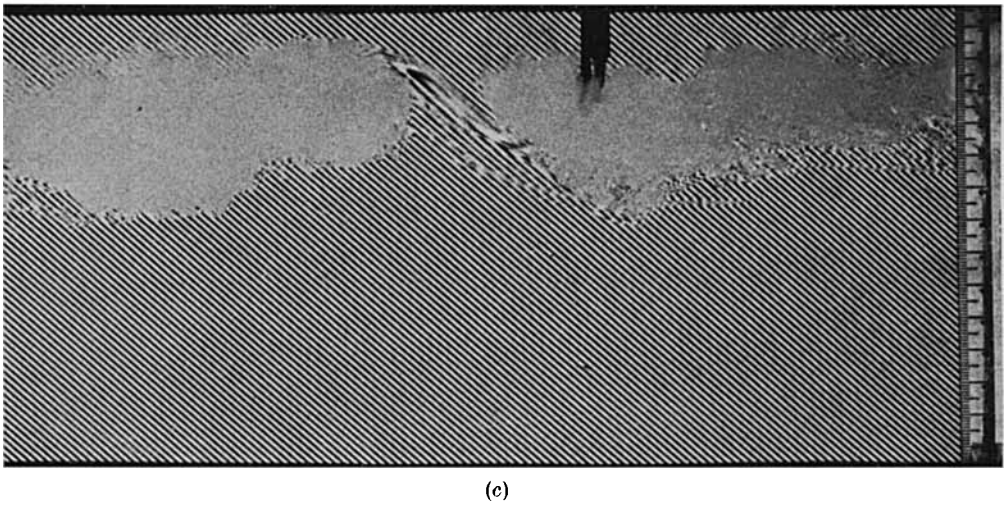

(*c*)

FIGURE 13. Photographs of the flow recorded in figure 12 at times (*a*) $\tau = 0$, (*b*) $\tau = 1{\cdot}0$, (*c*) $\tau = 2{\cdot}0$. The flow in the upper layer and direction of propagation of the billows are to the left.

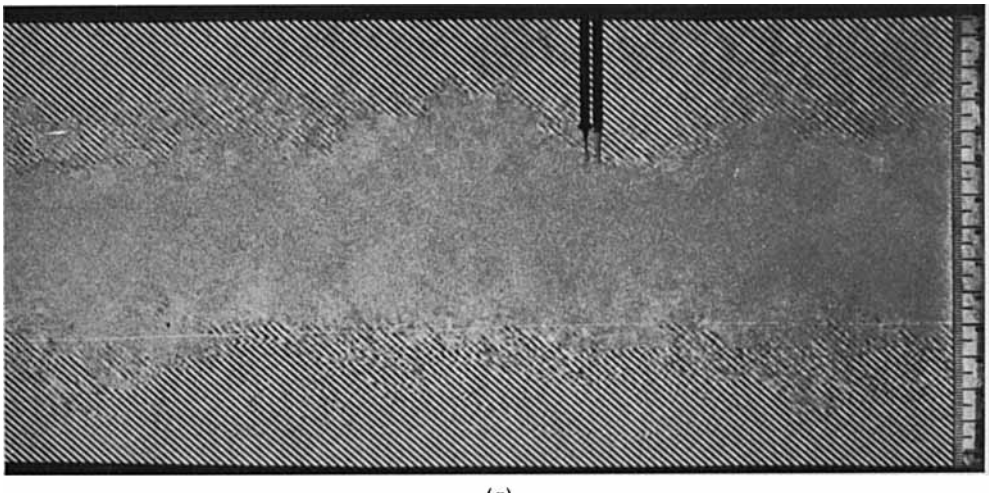

(*a*)

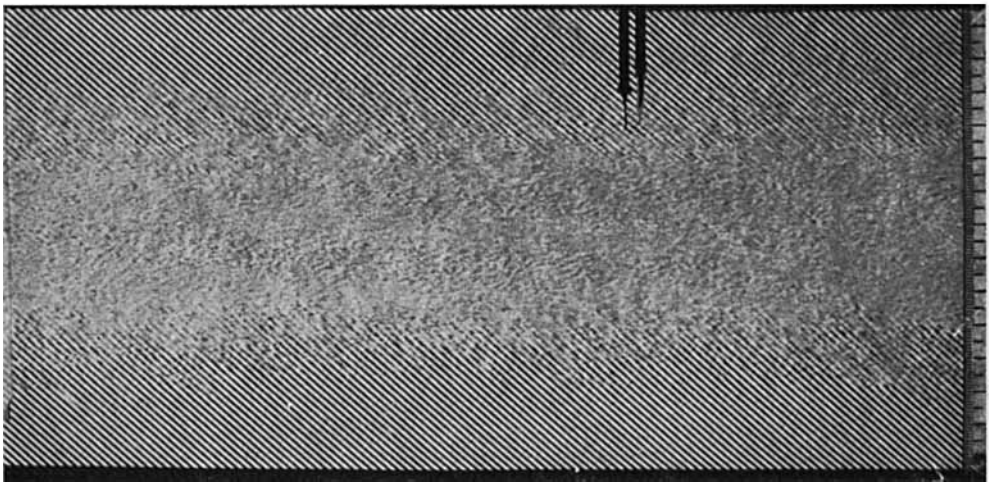

(*b*)

FIGURE 15. Photographs showing the appearance of the flow recorded by probes in figures 14(*a*) and (*b*) respectively. The flow in the upper layer is to the left.